annalen der physik
www.ann-phys.org

The Absorption Properties of One-Dimensional Spherical Photonic Crystals Based on Magnetized Ferrite Materials

*Tian-Qi Zhu, You-Ming Liu, Jia-Tao Zhang, and Hai-Feng Zhang**

Based on a spherical coordinate system and Maxwell's set of equations, the calculation formulas of one-dimensional (1-D) magnetized ferrite spherical photonic crystals (MFSPCs) are obtained and treated with the solution method of the spherical Bessel equations. Combined with the conventional transmission matrix method, expressions for the absorptance, reflectance, and transmittance of the 1-D MFSPCs are given. 1-D MFSPCs consisting of the general dielectric and Yttrium iron garnet (YIG) are also designed to verify the correctness of the conclusions. Variables such as external magnetic field, incidence angle, initial radius, and YIG thickness effects on the features of such 1-D MFSPCs are also discussed. The transformation of the external magnetic field has a linear relationship with the position of the absorption band (AB). The three variables of incidence angle, initial radius, and YIG thickness have a substantial influence on the width and position of the AB, which can be adjusted according to the actual demand and are of high application significance. The results of this study can be helpful for the design of multifunctional absorbers and radome.

1. Introduction

The problems of electromagnetic wave propagation in the dielectric layered structures have been a hot topic of research. Since the introduction of the concept of photonic crystals (PCs) in two seminal works by Yablonovitch and John,[1,2] PCs have become a research focus in the field of optics and electromagnetism. In 1989, Yablonovitch and Gmitter experimentally confirmed the existence of three-dimensional photonic energy band structures for the first time, further advancing the theoretical study of PCs. The unique optical properties of PCs have inspired scholars in the fields of photonics,[3] electronics,[4] and materials physics.[5] Based on their advantages of low propagation loss and reduced ohmic loss, PCs are important in waveguides,[6,7] sensors,[8] and absorbers.[9]

T.-Q. Zhu, J.-T. Zhang, H.-F. Zhang
College of Electronic and Optical Engineering & College of Flexible Electronics
Nanjing University of Posts and Telecommunications (NJUPT)
Nanjing 210023, P. R. China
E-mail: hanlor@njupt.edu.cn

Y.-M. Liu
Bell Honors School of Nanjing University of Posts and Telecommunication (NJUPT)
Nanjing 210023, P. R. China

The ORCID identification number(s) for the author(s) of this article can be found under https://doi.org/10.1002/andp.202200370

DOI: 10.1002/andp.202200370

The one-dimensional (1-D) PCs have the advantage of the simple periodic dielectric multilayer structure and simple fabrication, which occupy an important position in theoretical research. For the 1-D PCs, wave propagation properties can be analyzed and studied by acquainted with the transmission matrix method (TMM).[10] Based on the excellent properties of the 1-D PCs, scholars at home and abroad have conducted highly intensive research on them. At present, in addition to ordinary 1-D planar photonic crystals (PPCs), researchers also pay much attention to the relevant properties of the 1-D cylindrical photonic crystals (CPCs).[11–14] Extensive studies on the transmission properties of the 1-D CPCs using TMM.[15–18] The importance of the 1-D CPCs is increasing with the growing use of optical fibers[19] and optoelectronic components.[20] With the research and development of the 1-D CPCs, the field of spherical photonic crystals (SPCs) has also attracted the attention of numerous scholars. In 2016, Wendel and his team studied the unfolding of vector spherical waves in electromagnetic fields and obtained a complete set of radially independent amplitudes of vector spherical wave functions.[21] This study lays the foundation for the theoretical investigation of SPCs. The SPCs are important in optical displays,[22] millimeter wave communication,[23] nanomaterials,[24] and other fields. Since the 1-D SPCs are useful for broader physical applications compared with 1-D PPCs or 1-D CPCs, they have received widespread attention from scholars in the world, but the theoretical studies of their transmission characteristics are scarce. Under the magneto-optical effect, the 1-D magnetized ferrite spherical photonic crystals (MFSPCs) possess good magnetic tunability and excellent anisotropy, which have a promising future in the fabrication of multifunctional magnetically tunable absorbers,[25] optical circulators,[26] and filters.[27] Mehdian et al. investigated the magneto-optical properties and Faraday rotation effect of plasma-ferrite composite magneto-metamaterials and analyzed the variation pattern of the effective negative refractive index poles.[28] The magnitude of the negative effective refractive index pole varies with frequency, external magnetic field, and electron density of the plasma layer. The properties of ferrite materials have great potential for the development of waveguide circulators[29] and the design of tunable devices.[30] However, there are few studies on the 1-D SPCs that take full advantage of the superior magneto-optical properties of ferrite materials.

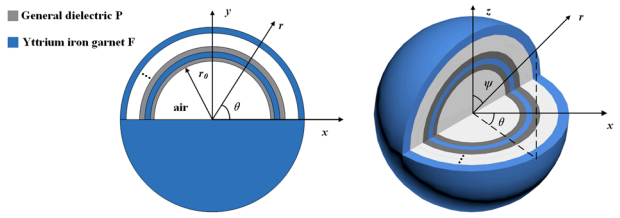

Figure 1. The model diagrams of the 1-D MFSPCs with periodic arrangement of the general dielectric and the YIG.

In this paper, based on the peculiarity that ferrite materials are anisotropic, the TMM is employed for the first time to derive the expressions for the transport properties of 1-D SPCs under the TE and TM polarization conditions. the 1-D MFSPCs are periodic structures consisting of a general dielectric and YIG. The effects of incidence angle, external magnetic field, initial radius, and YIG thickness on the absorption properties of the 1-D MFSPCs are investigated, which are important guidelines for the design of multipurpose absorbers and antenna protection. Furthermore, this paper only focuses on the theoretical study of the 1-D MFSPCs, and the specific implementation is still under study.

2. Simulation Model and Formulation

The structure of the 1-D MFSPCs is depicted in **Figure 1**. The given 1-D MFSPCs are made of the general dielectric (E) and the YIG (F) periodically arranged as $(EF)^N$, where N represents the number of periods. The initial radius r_0 is defined as 10 mm, the thickness of the general dielectric P d_A is 0.05 mm, and the thickness of F d_B is 2 mm. The effective refractive index of the general dielectric P is $n_P = 4$, and the effective magnetic permeability of F will be described in detail below.

Due to the special geometric properties of the sphere, inspired by the idea of the micro-element method and the definition of the incidence angle under the CPCs,[14] the incidence angle, TE and TM waves are defined by taking the profile of the spherical wave and 1-D MFSPCs parallel to the wave propagation direction, as shown in **Figure 2**. For this plane, the electric field E is perpendicular to the plane, the magnetic field H is parallel to the plane, and the wave vector $\boldsymbol{k}$ indicates the propagation direction. And after considering the relationship between r, θ, and Ψ with the plane, define the electric field E in the TE wave as $E = (0, E_\theta, 0)$ and the magnetic field H as $H = (H_r, 0, H_\varphi)$. By analogy, for the TM modes, the electric field E takes the form of $E = (E_r, 0, E_\varphi)$ and the magnetic field H takes the form of $H = (0, H_\theta, 0)$.

Based on the above description for TE and TM waves, the incidence angle can be defined. Since both spherical waves and 1-D MFSPCs are spherical objects, they cannot be described by the conventional way of determining the angle of incidence by planes. It is straightforward to associate that when dealing with curved surfaces, we often use tangents to stipulate the angles. Combining the above factors, it is chosen to utilize the cross section where the spherical wave and 1-D MFSPCs intersect to define the angle of incidence γ. The intersection of the cross-section of the spherical wave and the 1-D MFSPCs is taken as the vertex of the angle, and the tangents of the spherical wave cross-section and the 1-D MFSPCs cross-section out of the intersection are made respectively. The angle made by the two tangents is the angle of incidence.

In the presence of a high-frequency magnetic field, the spin electron magnetic moment does not necessarily move in phase with the external magnetic field. In this case, the internal magnetization strength M of any ferromagnetic material is not necessarily parallel or in-phase with the applied magnetic field H. The total magnetic field strength can be expressed as[31,32]:

$$B = \mu_0 H + M \tag{1}$$

In the meantime, M can be expressed in terms of H. Therefore, Equation (1) can be rewritten as:

$$B = \mu_m H \tag{2}$$

Therefore, μ_m can be obtained by establishing the conversion relation between B and H. In the Cartesian coordinate system, x, y and z are satisfied $x \times y = z$. However, in the spherical

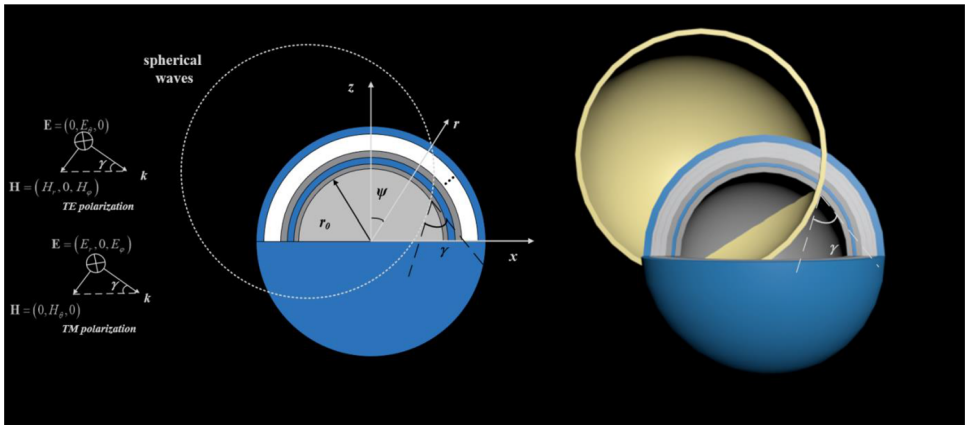

Figure 2. The main view and diagrammatic figure of 1-D MFSPCs with the incidence angle, electromagnetic direction and magnetic field direction indicated in detail.

coordinate system, r, θ and ψ are fulfilled $r \times \theta = \psi$, so the form of μ_m in the spherical coordinate system can be acquired by the form of the YIG permeability tensor expression under transverse magnetization in the Cartesian coordinate system. Due to the different forms of the decomposition of M in r, θ and ψ, B, and H present the following relationship.

$$B_r = \mu_r H_r + j\mu_k H_\varphi \tag{3a}$$

$$B_\theta = \mu_0 H_\theta \tag{3b}$$

$$B_\varphi = -j\mu_k H_r + \mu_r H_\varphi \tag{3c}$$

Thus the expression for μ_m of YIG in the spherical coordinate system is obtained as:

$$\mu_m = \begin{pmatrix} \mu_r & 0 & i\mu_k \\ 0 & \mu_0 & 0 \\ -i\mu_k & 0 & \mu_r \end{pmatrix} \tag{4}$$

$$\mu_r = 1 + \frac{\omega_m(\omega_0 - i\eta\omega)}{(\omega_0 - i\eta\omega)^2 - \omega^2} \tag{5a}$$

$$\mu_k = \frac{\omega_m \omega}{(\omega_0 - i\eta\omega)^2 - \omega^2} \tag{5b}$$

Here, $\omega_m = 2\pi f_m$ is the circular frequency with $f_m = 2.8 \times 10^6 \times M_s$, where M_s is the saturation magnetization equal to 1780 Oe. $\omega_0 = 2\pi f_0$ is the resonance frequency with $f_0 = 2.8 \times 10^6 \times H_0$, for which H_0 is the external magnetic field and ω_0 is associated with H_0. In addition, $\eta = 0.002$ is the damping constant and the dielectric constant of the ferrite material $\epsilon_m = 15$.[33]

The effective permeability and effective refractive index of the YIG in the TE waves can be written as $\mu_{eff} = [\mu_r^2 + (i\mu_k)^2]/\mu_r$ and $n_{TE} = \sqrt{[\varepsilon_m(\mu_r{}^2 + (j\mu_k)^2)]/\mu_r}$, severally. Due to the ferrite material is not susceptible to the TM waves, the effective permeability and effective refractive index of the YIG in the TM waves can be formulated as μ_0 and $n_{TM} = \sqrt{\varepsilon_m \cdot \mu_0}$, separately.[33]

The time-dependent Maxwell's equations can be expressed in the following form:

$$\nabla \times E = -\mu_0 \mu_m \frac{\partial H}{\partial t} \tag{6}$$

$$\nabla \times H = \varepsilon_0 \varepsilon_m \frac{\partial E}{\partial t} \tag{7}$$

Considering the TE waves, the electric and magnetic fields are protrayed as:

$$E = \left(0, E_\theta, 0\right) e^{-i\omega t} \tag{8}$$

$$H = \left(H_r, 0, H_\varphi\right) e^{-i\omega t} \tag{9}$$

The studied spherical waves are simple harmonics, and the field quantities all vary with time at a certain angular frequency according to the sinusoidal law, so the wave components in the three directions can be expressed in complex form, and the use of complex arithmetic law can reduce the time order and eliminate the time factor. The influence of time on the electric and magnetic field components can be disregarded in the derivation of the formula, which facilitates mathematical calculation. Considering the propagation of the diverging or converging spherical waves, the derivative with respect to ψ can be omitted. Substituting the above equation into Maxwell's system of equations to expand, the following equation is obtained.

$$\frac{1}{r^2 \sin\theta} \frac{\partial}{\partial \varphi}\left(rE_\theta\right) = i\omega\mu_0 \left(\mu_r H_r + i\mu_k H_\varphi\right) \tag{10}$$

$$\frac{1}{r}\left[\frac{\partial}{\partial r}\left(rE_\theta\right)\right] = i\omega\mu_0 \left(i\mu_k H_r - \mu_r H_\varphi\right) \tag{11}$$

$$\frac{1}{r\sin\theta}\left[\frac{\partial H_r}{\partial \varphi} - \frac{\partial}{\partial r}\left(r\sin\theta H_\varphi\right)\right] = i\omega\varepsilon_0\varepsilon_m E_\theta \tag{12}$$

Then get,

$$H_\varphi = \frac{1}{\mu_r^2 - \mu_k^2} \cdot \frac{1}{i\omega\mu_0 r}\left[\frac{i\mu_k}{r\sin\theta}\frac{\partial}{\partial\varphi}\left(rE_\theta\right) - \mu_r \frac{\partial}{\partial r}\left(rE_\theta\right)\right] \tag{13}$$

$$H_r = \frac{1}{\mu_r^2 - \mu_k^2} \cdot \frac{1}{i\omega\mu_0 r}\left[i\mu_k \frac{\partial}{\partial r}\left(rE_\theta\right) + \frac{\mu_r}{r\sin\theta}\frac{\partial}{\partial\varphi}\left(rE_\theta\right)\right] \tag{14}$$

Then substitute Equations (13) and (14) into Equation (11) and bond the above results to obtain the equation expression of E_θ as follows:

$$\frac{1}{r^2}\frac{\partial}{\partial r}\left(r^2 \frac{\partial E_\theta}{\partial r}\right) + \frac{1}{r^2 \sin^2\theta}\frac{\partial^2 E_\theta}{\partial \varphi^2} + k^2 E_\theta = 0 \tag{15}$$

Worthy of mention is that, considering the field generated by TE polarization, the wave vector $\boldsymbol{k}$ in Equation (15) is shown as $\omega\sqrt{\varepsilon_0\varepsilon_m\mu_0\mu_{eff}} \cdot \cos\gamma$, where γ indicates the incident angles of the surfaces.

Define $E_\theta(x) = V(x)\Psi(\varphi)$, where $x = kr$. It is toilless to be convinced of that the angular part of E_θ meets the following equation:

$$\frac{d^2\Psi}{d\varphi^2} + m^2\varphi = 0 \tag{16}$$

Taking full advantage of the properties of the differential equation can yield $\Psi \sim e^{im\varphi}$, for which m can be positive integers, zero and negative integers.

Let

$$m^2 = l(l+1)\sin^2\theta \tag{17}$$

Concatenating Equations (15), (16), and (17), the equation on $V(x)$ can be adapted to a standard spherical Bessel equation.

$$x^2\frac{d^2V}{dx^2} + x\frac{dV}{dx} + \left[x^2 - \left(l + \frac{1}{2}\right)^2\right]V(x) = 0 \tag{18}$$

$V(x)$ can be indicated by a linear combination of solutions of the standard spherical Bessel equation.

$$V(x) = Aj_l(x) + Bn_l(x) \tag{19}$$

where $j_l(x)$ and $n_l(x)$ are semi-odd order Bessel functions, which are composite functions of power and trigonometric functions. In the case with spherical waves, the specific expressions of $j_l(x)$ and $n_l(x)$ are shown below:

$$\begin{aligned} j_l(x) &= \sqrt{\frac{\pi}{2x}} J_{l+\frac{1}{2}}(x) \\ n_l(x) &= \sqrt{\frac{\pi}{2x}} N_{l+\frac{1}{2}}(x) \end{aligned} \tag{20}$$

For simplicity, $U(x)$ is represented as:

$$U(x) = -\frac{1}{i\omega\mu_0 r}\frac{\partial}{\partial x}[xV(x)] = -\frac{1}{i\omega\mu_0 r}\left[V(x) + x\frac{\partial V(x)}{\partial x}\right] \tag{21}$$

Substitute Equation (19) into Equation (21)

$$U(x) = -\frac{1}{i\omega\mu_0 r}\left[Aj_l(x) + Bn_l(x) + xAj_l'(x) + xBn_l'(x)\right] \tag{22}$$

Here, $j_l'(x)$ and $n_l'(x)$ are the first order derivatives of the semi-odd Bessel functions, and the corresponding equations are written as:

$$\begin{aligned} j_l'(x) &= \sqrt{\frac{\pi}{2x}} J'_{l+\frac{1}{2}}(x) - \frac{1}{2}\sqrt{\frac{\pi}{2}} x^{-\frac{3}{2}} J_{l+\frac{1}{2}}(x) \\ n_l'(x) &= \sqrt{\frac{\pi}{2x}} N'_{l+\frac{1}{2}}(x) - \frac{1}{2}\sqrt{\frac{\pi}{2}} x^{-\frac{3}{2}} N_{l+\frac{1}{2}}(x) \end{aligned} \tag{23}$$

To correlate the 1-D SPCs at different radii, the TMM is put into use. We define a set of vectors $\begin{pmatrix} V(x) \\ U(x) \end{pmatrix}$ and make it possible to link them with vectors at other radii by calculating the homologous transmission matrix. Presume that the initial radius is r_0 and $x_0 = kr_0$

$$\begin{pmatrix} V(x) \\ U(x) \end{pmatrix} = \mathrm{M}\begin{pmatrix} V(x_0) \\ U(x_0) \end{pmatrix} = \begin{pmatrix} M_{11} & M_{12} \\ M_{21} & M_{22} \end{pmatrix}\begin{pmatrix} V(x_0) \\ U(x_0) \end{pmatrix} \tag{24}$$

This matrix equation has the capability to connect two non-zero magnetic fields at two different radial positions r_0 and r. Taking special values for $V(x)$ and $U(x)$ is a decent way to earn the elements of the transmission matrix M.

For the purpose of further predigesting the calculation, first we assume that:

$$\begin{aligned} V(x_0) &= 1 \\ U(x_0) &= 0 \end{aligned} \tag{25}$$

Therefore, coalescing the knowledge of matrix calculation, it can be overtly obtained the detailed expression of M_{11} and M_{21}.

$$M_{11} = V(x) = Aj_l(x) + Bn_l(x) \tag{26}$$

$$M_{21} = U(x) = -\frac{1}{i\omega\mu_0 r}\left[Aj_l(x) + Bn_l(x) + xAj_l'(x) + xBn_l'(x)\right] \tag{27}$$

The special values of $V(x)$ and $U(x)$ to determine the expressions for A and B. Substituting Equations (19) and (22) into Equation (25), the following results can be gotten:

$$\begin{aligned} V(x_0) &= Aj_l(x_0) + Bn_l(x_0) = 1 \\ U(x_0) &= Aj_l(x_0) + Bn_l(x_0) + x_0 Aj_l'(x_0) + x_0 Bn_l'(x_0) = 0 \end{aligned} \tag{28}$$

The values of A and B are as follows:

$$\begin{aligned} A &= \frac{1}{j_l(x_0)n'_l(x_0) - n_l(x_0)j_l'(x_0)}\left[n_l'(x_0) + \frac{n_l(x_0)}{x_0}\right] \\ B &= \frac{1}{n_l(x_0)j_l'(x_0) - n'_l(x_0)j_l(x_0)}\left[j_l'(x_0) + \frac{j_l(x_0)}{x_0}\right] \end{aligned} \tag{29}$$

Consequently, the constant terms of M_{11} and M_{21} in the transmission matrix M are solved and Equations (26) and (27) are rewritten as:

$$M_{11} = \frac{j_l(x)}{j_l(x_0)n'_l(x_0) - n_l(x_0)j_l'(x_0)}\left[n_l'(x_0) + \frac{n_l(x_0)}{x_0}\right] + \frac{n_l(x)}{n_l(x_0)j_l'(x_0) - n'_l(x_0)j_l(x_0)}\left[j_l'(x_0) + \frac{j_l(x_0)}{x_0}\right] \tag{30}$$

$$\begin{aligned} M_{21} = -\frac{1}{i\omega\mu_0 r}\Bigg\{ &\frac{j_l(x)}{j_l(x_0)n'_l(x_0) - n_l(x_0)j_l'(x_0)}\left[n_l'(x_0) + \frac{n_l(x_0)}{x_0}\right] + \frac{n_l(x)}{n_l(x_0)j_l'(x_0) - n'_l(x_0)j_l(x_0)}\left[j_l'(x_0) + \frac{j_l(x_0)}{x_0}\right] \\ &+ \frac{xj_l'(x)}{j_l(x_0)n'_l(x_0) - n_l(x_0)j_l'(x_0)}\left[n_l'(x_0) + \frac{n_l(x_0)}{x_0}\right] + \frac{xn_l'(x)}{n_l(x_0)j_l'(x_0) - n'_l(x_0)j_l(x_0)}\left[j_l'(x_0) + \frac{j_l(x_0)}{x_0}\right]\Bigg\} \end{aligned} \tag{31}$$

Then, $V(x)$and $U(x)$are assigned the values to:

$$\begin{aligned} V\left(x_0\right) &= 0 \\ U\left(x_0\right) &= 1 \end{aligned} \tag{32}$$

Cushy to get:

$$M_{12} = V(x) = Cj_1(x) + Dn_1(x) \tag{33}$$

$$M_{22} = U(x) = -\frac{1}{i\omega\mu r}\left[Cj_1(x) + Dn_1(x) + xCj_1'(x) + xDn_1'(x)\right] \tag{34}$$

Similar to the solving for A and B, substituting Equations (19) and (22) to Equation (32).

$$V\left(x_0\right) = Cj_1\left(x_0\right) + Dn_1\left(x_0\right) = 0$$

$$U\left(x_0\right) = -\frac{1}{i\omega\mu_0 r_0}\left[Cj_1\left(x_0\right) + Dn_1\left(x_0\right) + x_0 Cj_1'\left(x_0\right) + x_0 Dn_1'\left(x_0\right)\right] = 1 \tag{35}$$

The values of C and D are indicated below:

$$\begin{aligned} C &= \frac{1}{n_1\left(x_0\right)j_1'\left(x_0\right) - n'_1\left(x_0\right)j_1\left(x_0\right)}\left[-\frac{i\omega\mu_0}{k}n_1\left(x_0\right)\right] \\ D &= \frac{1}{j_1\left(x_0\right)n'_1\left(x_0\right) - n_1\left(x_0\right)j_1'\left(x_0\right)}\left[-\frac{i\omega\mu_0}{k}j_1\left(x_0\right)\right] \end{aligned} \tag{36}$$

The values of C and D are then brought into Equations (33) and (34) to calculate $M_{12}$and M_{22} in the transmission matrix.

$$\begin{aligned} M_{12} = {} & \frac{j_1(x)}{n_1\left(x_0\right)j_1'\left(x_0\right) - n'_1\left(x_0\right)j_1\left(x_0\right)}\left[-\frac{i\omega\mu_0}{k}n_1\left(x_0\right)\right] \\ & + \frac{n_1(x)}{j_1\left(x_0\right)n'_1\left(x_0\right) - n_1\left(x_0\right)j_1'\left(x_0\right)}\left[-\frac{i\omega\mu_0}{k}j_1\left(x_0\right)\right] \end{aligned} \tag{37}$$

$$\begin{aligned} M_{22} = -\frac{1}{i\omega\mu_0 r}\Bigg\{ & \frac{j_1(x)}{n_1\left(x_0\right)j_1'\left(x_0\right) - n'_1\left(x_0\right)j_1\left(x_0\right)}\left[-\frac{i\omega\mu_0}{k}n_1\left(x_0\right)\right] \\ & + \frac{n_1(x)}{j_1\left(x_0\right)n'_1\left(x_0\right) - n_1\left(x_0\right)j_1'\left(x_0\right)}\left[-\frac{i\omega\mu_0}{k}j_1\left(x_0\right)\right] \\ & + \frac{xj_1'(x)}{n_1\left(x_0\right)j_1'\left(x_0\right) - n'_1\left(x_0\right)j_1\left(x_0\right)}\left[-\frac{i\omega\mu_0}{k}n_1\left(x_0\right)\right] \\ & + \frac{xn_1'(x)}{j_1\left(x_0\right)n'_1\left(x_0\right) - n_1\left(x_0\right)j_1'\left(x_0\right)}\left[-\frac{i\omega\mu_0}{k}j_1\left(x_0\right)\right]\Bigg\} \end{aligned} \tag{38}$$

At this point, the transmission matrix of the 1-D SPCs is derived, and when the electromagnetic wave propagates the 1-D SPCs, the input and output magnetic fields can be contacted by the total transmission matrix of the structure. If the TM polarization is performed, the elements of the transmission matrix $M_2 = \begin{pmatrix} m_{11} & m_{12} \\ m_{21} & m_{22} \end{pmatrix}$ take a similar form as Equations (30), (31), (37) and (38) by simply replacing $-\mu$ with ϵ. m_{11}, m_{21}, m_{12}, and m_{22} are written as:

$$m_{11} = \frac{j_1(x)}{j_1\left(x_0\right)n'_1\left(x_0\right) - n_1\left(x_0\right)j_1'\left(x_0\right)}\left[n_1'\left(x_0\right) + \frac{n_1\left(x_0\right)}{x_0}\right] + \frac{n_1(x)}{n_1\left(x_0\right)j_1'\left(x_0\right) - n'_1\left(x_0\right)j_1\left(x_0\right)}\left[j_1'\left(x_0\right) + \frac{j_1\left(x_0\right)}{x_0}\right] \tag{39}$$

$$\begin{aligned} m_{21} = \frac{1}{i\omega\varepsilon r}\Bigg\{ & \frac{j_1(x)}{j_1\left(x_0\right)n'_1\left(x_0\right) - n_1\left(x_0\right)j_1'\left(x_0\right)}\left[n_1'\left(x_0\right) + \frac{n_1\left(x_0\right)}{x_0}\right] + \frac{n_1(x)}{n_1\left(x_0\right)j_1'\left(x_0\right) - n'_1\left(x_0\right)j_1\left(x_0\right)}\left[j_1'\left(x_0\right) + \frac{j_1\left(x_0\right)}{x_0}\right] \\ & + \frac{xj_1'(x)}{j_1\left(x_0\right)n'_1\left(x_0\right) - n_1\left(x_0\right)j_1'\left(x_0\right)}\left[n_1'\left(x_0\right) + \frac{n_1\left(x_0\right)}{x_0}\right] + \frac{xn_1'(x)}{n_1\left(x_0\right)j_1'\left(x_0\right) - n'_1\left(x_0\right)j_1\left(x_0\right)}\left[j_1'\left(x_0\right) + \frac{j_1\left(x_0\right)}{x_0}\right]\Bigg\} \end{aligned} \tag{40}$$

$$m_{12} = \frac{j_1(x)}{n_1\left(x_0\right)j_1'\left(x_0\right) - n'_1\left(x_0\right)j_1\left(x_0\right)}\left[\frac{i\omega\varepsilon}{k}n_1\left(x_0\right)\right] + \frac{n_1(x)}{j_1\left(x_0\right)n'_1\left(x_0\right) - n_1\left(x_0\right)j_1'\left(x_0\right)}\left[\frac{i\omega\varepsilon}{k}j_1\left(x_0\right)\right] \tag{41}$$

$$\begin{aligned} m_{22} = \frac{1}{i\omega\varepsilon r}\Bigg\{ & \frac{j_1(x)}{n_1\left(x_0\right)j_1'\left(x_0\right) - n'_1\left(x_0\right)j_1\left(x_0\right)}\left[\frac{i\omega\varepsilon}{k}n_1\left(x_0\right)\right] + \frac{n_1(x)}{j_1\left(x_0\right)n'_1\left(x_0\right) - n_1\left(x_0\right)j_1'\left(x_0\right)}\left[\frac{i\omega\varepsilon}{k}j_1\left(x_0\right)\right] \\ & + \frac{xj_1'(x)}{n_1\left(x_0\right)j_1'\left(x_0\right) - n'_1\left(x_0\right)j_1\left(x_0\right)}\left[\frac{i\omega\varepsilon}{k}n_1\left(x_0\right)\right] + \frac{xn_1'(x)}{j_1\left(x_0\right)n'_1\left(x_0\right) - n_1\left(x_0\right)j_1'\left(x_0\right)}\left[\frac{i\omega\varepsilon}{k}j_1\left(x_0\right)\right]\Bigg\} \end{aligned} \tag{42}$$

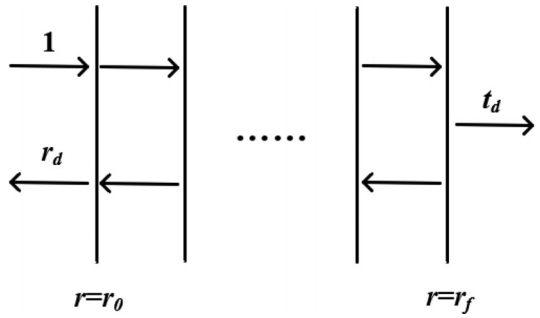

Figure 3. The schematic diagram of spherical wave propagation at positive incidence, where the surface interface is intentionally drawn as a straight line for ease of illustration.

However, for wave propagation, it is convenient to represent the field as the sum of two opposite propagating waves, which is the superposition of the incident and outgoing waves. To meet the computational requirements, these two waves are generally expressed by two Hankel functions:

$$\begin{aligned} h_1^{(1)}(x) &= j_1(x) + in_1(x) \\ h_1^{(2)}(x) &= j_1(x) - in_1(x) \end{aligned} \tag{43}$$

For the TE waves, the electric and magnetic fields are decomposed into the incident and outgoing directions, which are written as the following expressions:

$$\begin{aligned} E_\theta^+(x) &= Qh_1^{(2)}(x)\, e^{\mathrm{i}m\varphi} \\ E_\theta^-(x) &= Ph_1^{(1)}(x)\, e^{\mathrm{i}m\varphi} \end{aligned} \tag{44}$$

For the sake of observation and understanding, the discussion here focuses on the case when $\gamma = 0$. By defining the incident spherical wave as 1 and analogizing it to Airy's formula in the plane, the outgoing spherical wave can be expressed by the transmission coefficient t_d and the reflected spherical wave by the reflection coefficient r_d. At the same time, the expression of the transmission matrix of each layer after the incident spherical wave can be readily obtained by utilizing the TMM, which makes the propagation of the spherical wave in 1-D MFSPCs regular. It is therefore associated that the TMM can be combined with the propagation model of **Figure 3** to obtain expressions for r_d and t_d.[15]

Further, it is not possible to solve for the rd and td variables by the electric or magnetic field equations alone. Notice that the electric and magnetic fields can be related to each other using the Hankel function as follows.

$$H_\varphi^+(x) = -\frac{QC_1^{(2)}(x)}{i\omega\mu_0 r} E_\theta^+(x) e^{\mathrm{i}m\varphi} \tag{45}$$

$$H_\varphi^-(x) = -\frac{PC_1^{(1)}(x)}{i\omega\mu_0 r} E_\theta^-(x) e^{\mathrm{i}m\varphi} \tag{46}$$

where,

$$\begin{aligned} C_1^{(2)}(x) &= 1 + x\frac{h_1^{(2)\prime}(x)}{h_1^{(2)}(x)} \\ C_1^{(1)}(x) &= 1 + x\frac{h_1^{(1)\prime}(x)}{h_1^{(1)}(x)} \end{aligned} \tag{47}$$

Integrating the above analysis and referring to the structure of Figure 1, the outgoing wave is incident to the $r = r_0$ interface and ultimately exits from the $r = r_f$ interface. The electric and magnetic fields at r_0 and r_f are denoted singly. On account, TMM can concatenate 1-D SPCS of different radii, the reflection coefficient r_d, and transmission coefficient t_d can be characterized by the elements in the transmission matrix M.

$$\begin{pmatrix} 1 + r_d \\ -\frac{C_1^{(2)}(x_0)}{i\omega\mu_0 r_0} - \frac{C_1^{(1)}(x_0)}{i\omega\mu_0 r_0} r_d \end{pmatrix} = M^{-1} \begin{pmatrix} t_d \\ -\frac{C_1^{(2)}(x_f)}{i\omega\mu_0 r_f} t_d \end{pmatrix} \tag{48}$$

where

$$\begin{aligned} M &= M_1 M_2 M_1 \ldots M_2 M_1 M_2 \\ M^{-1} &= \begin{pmatrix} M'_{11} & M'_{12} \\ M'_{21} & M'_{22} \end{pmatrix} \end{aligned} \tag{49}$$

The basic knowledge of matrices is applied to Equation (41). Synthesizing the above results, we determine the expressions for the reflection and transmission coefficients r_d and t_d.

$$t_d = \frac{C_1^{(1)}(x_0) - C_1^{(2)}(x_0)}{i\omega\mu_0 r_0 \left[M'_{11} \frac{C_1^{(1)}(x_0)}{i\omega\mu_0 r_0} M'_{21} - \frac{C_1^{(2)}(x_f)}{i\omega\mu_0 r_f} \cdot \frac{C_1^{(1)}(x_0)}{i\omega\mu_0 r_0} M'_{12} - M'_{22} \frac{C_1^{(2)}(x_f)}{i\omega\mu_0 r_f} \right]} \tag{50}$$

$$r_d = \left[M'_{11} - M'_{12} \frac{C_1^{(2)}(x_f)}{i\omega\mu_0 r_f} \right] t_d - 1 \tag{51}$$

Moreover, combining the above theoretical treatment, the absorptance (A_b), transmittance (T), and reflectance (R) of 1-D MFSCPs are completely deduced.

$$T = |t_d|^2 R = |r_d|^2 \tag{52}$$

$$A_b = 1 - T - R \tag{53}$$

3. Analysis and Discussion

The absorption, reflection, and transmission spectra of the 1-D MFSPCs under the TE modes and TM modes are exhibited in **Figure 4**, where γ is 75°, r_0 is 1 mm, H_0 is 6500 Oe, $d_A = 0.05$ mm, and $d_B = 2$ mm. It is apparent that in the TM waves, the refractive index of YIG is a definite constant independent of frequency owing to the absence of interaction between the TM waves and the ferrite material. Therefore, under the TM polarization, YIG is treated as a general metallic material and the absorptance and reflectance expressions are derived in combination with TMM. Based on the absorption and reflection spectra of the TM waves in Figure 4, it is effortless to detect that the 1-D MFSPCs have similar transmission properties to 1-D SPCs composed of a general dielectric, and emerge as a comb of spectral lines. Ulteriorly, the spectra of TE polarization are analyzed. The YIG is an anisotropic material whose magnetic permeability is tensor under the action of an external magnetic field. Therefore, the refractive index of the YIG varies with frequency in the TE waves. From Figure 4, it

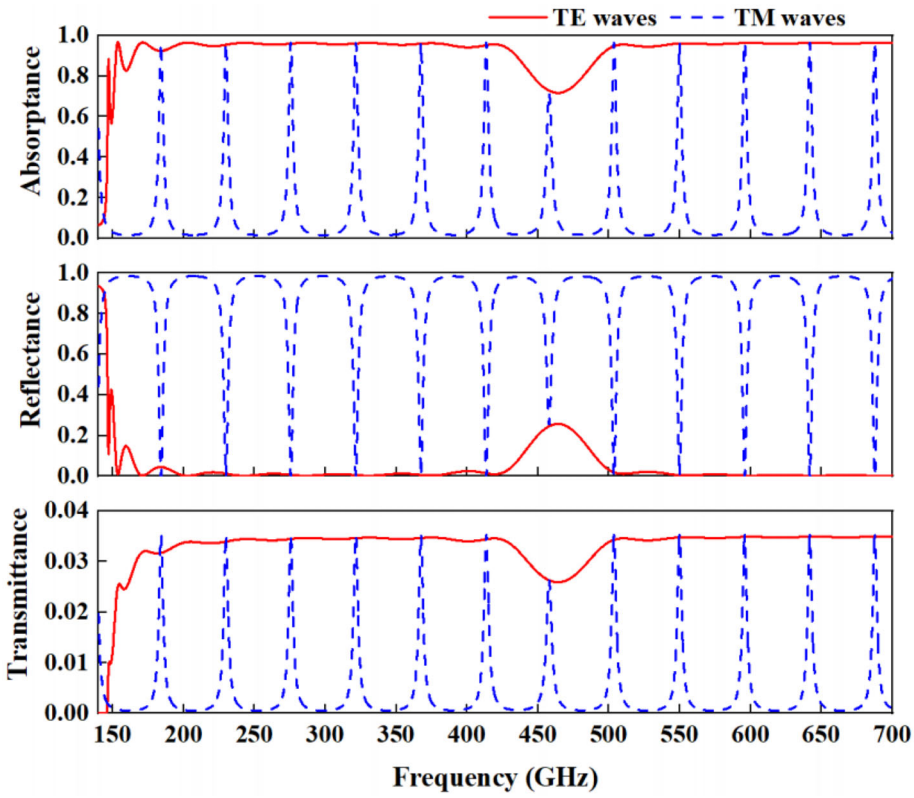

Figure 4. The absorption and reflection spectra of the TE and TM waves at $\gamma = 75°$, $r_0 = 1$ mm, $d_A = 0.05$ mm, $d_B = 2$ mm, and the external magnetic field $H_0 = 6500$ Oe.

is observed in a breeze that 1-D MFSPCs form multiple absorption bands (ABs) in the 150–700 GHz. Noteworthy, the refractive index of the YIG mutates in particular frequency ranges,[34] and the intensity and frequency band of the mutation are hinged on the external magnetic field. Meanwhile, an AB extends from 164.7 to 434.6 GHz. It coincides with the band where YIG refractive index saltates. Therefore, it is inferred that the formation of the AB in the 164.7–434.6 GHz band is related to the refractive index change of YIG. Electromagnetic waves in this frequency band can be absorbed by such 1-D MFSPCs. Scanning the transmission spectrum, it is apparent that the transmittance is close to 0 and fluctuates fantastically trifling under the TE mode. However, the transmittance spectrum under TM polarization is comb-shaped and the peak points are identical to the absorption one, which leads to the conclusion that the alteration of transmittance is caused by the mutual effect of absorptance and reflectance. Undoubtedly, the presented 1-D MFSPCs show different absorption features in the TE and TM waves, which are related to the features of YIG.

Thanks to the tunable nature of YIG under the magneto-optical effect, the change of the external magnetic field affects the absorption spectra of the 1-D MFSPCs. It is deduced from **Figure 5** that the effects of the external magnetic field on the ABs are dominantly in the frequency band position. The absorption curves plotted for H_0 are 6000, 6250, 6500, and 7000 Oe with $\gamma = 75°$, $r_0 = 1$ mm, $d_A = 0.05$ mm, and $d_B = 2$ mm. The ABs of the 1-D MFSPCs shift toward the high-frequency region with the enlargement of H_0. According to the following pictures, it can

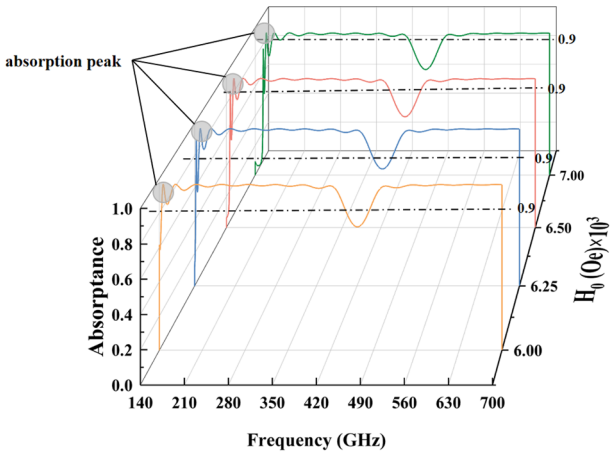

Figure 5. The impacts of H_0 on the absorption spectra of the TE waves at $\gamma = 75°$, $r_0 = 1$ mm, $d_A = 0.05$ mm, and $d_B = 2$ mm.

be comprehended that the absorption peak exists at 146.1 GHz for $H_0 = 6000$ Oe, with a maximum absorptance of 0.96. Simultaneously, an AB is generated between 158.4 and 434.2 GHz. At $H_0 = 6250$ Oe, the absorption peak is readily detected at 149.9 GHz and the AB is positioned in the 161.4–434.44 GHz band. If $H_0 = 6500$ Oe, the appearance of the absorption peak can be noticed at 153.6 GHz, where the peak of the absorption is $\simeq H_0 = 6000$ Oe. The AB also moves toward the higher frequen-

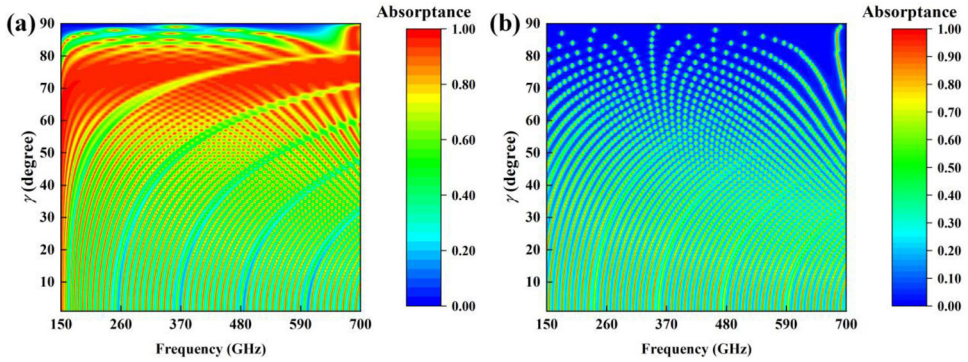

Figure 6. The absorption spectra when $r_0 = 1$ mm, $d_A = 0.05$ mm, $d_B = 2$ mm, and $H_0 = 6500$ Oe. a) The influences of incident angle γ on absorption under the TE polarization, b) the effects of incident angle γ variation on absorption under the TM polarization.

cies and includes the region from 164.7 to 434.6 GHz. Similarly, defining $H_0 = 7000$ Oe, the absorption peak occurs at 161.3 GHz and the AB is located in the 171.3–435.1 GHz band. Overall, the 1-D MFSPCs have exceptional tunability, making it possible to shift the ABs to high-frequency interval by enhancing the external magnetic field.

Figure 6 gives the absorption spectra when $r_0 = 1$ mm, $d_A = 0.05$ mm, $d_B = 2$ mm, and $H_0 = 6500$ Oe for the angle change from 0° to 90°. For the TE waves, an AB can be formed when γ is in the range of 65° to 80°. The AB is broad near the $\gamma = 75°$, and the absorptance of the 1-D MFSPCs gradually descends when γ is larger than 80°. When $\gamma = 89°$, the absorptance is ≈0. Figure 6a shows that a wider AB can be formed by appropriately raising γ under the TE polarization conditions, which can achieve remarkable performance with more than 90% of electromagnetic waves being absorbed. A larger incidence angle is indispensable for the formation of an ultra-wide AB.

It is manifest from Figure 6b that the absorption spectra of the 1-D MFSPCs between $\gamma = 0°$ and $\gamma = 50°$ have similar trends to those under the TE polarization. When γ is small, neither the TE polarization nor the TM one can form the expansive ABs, so the absorption spectra under the two conditions are somewhat comparable. When γ continues to increase, unlike the extremely broad ABs formed under the TE polarization, the 1-D MFSPCs in the TM waves form absorption peaks, and the number of absorption peaks is negatively correlated with γ. When γ is equal to 89°, the number of absorption peaks is the least. The reason why the TE and TM waves show distinct differences in absorption spectra under the variation of γ is that the magnetic dipole of YIG interacts only with TE waves, satisfying the needs of diverse physical scenarios.

Figure 7 depicts the angular variation profiles for adjusting the media thickness with $r_0 = 1$ cm and $H_0 = 6500$ Oe, where a) $d_A = 0.05$ mm, $d_B = 2$ mm in the figure, b) $d_A = 0.05$ mm, $d_B = 2$ mm is set in the figure, c) $d_A = 0.05$ mm, $d_B = 2$ mm in the figure, d) $d_A = 0.05$ mm, $d_B = 2$ mm is specified. From Figure 7a–c, between $\gamma = 0$–50°, there is no emblematic AB formation, and a wide variety of absorption peaks can be perceived. It is also undemanding to observe that the absorption spectra are characterized by periodic and the range of periodic frequencies narrows and accrues in number as the d_B enlarges. A striking difference occurs when γ is between 65° and 80°, the ABs can be formed in the 1-D MFSPCs of all three cases, but the bandwidths of the ABs become narrower when the YIG thickness increases. From Figure 7d, it can be seen that the absorptance is considerably affected when d_B decreases. The maximum absorptance is only 60% which generates large amounts of energy dissipation. Neither ABs nor absorption peaks appear, and the vast majority of electromagnetic waves are not absorbed by the 1-D MFSPCs. Therefore, it can be deduced that the proper d_B is the key to ensuring the superior absorption performance of the 1-D MFSPCs.

In the following, attention is turned to the initial radius, when $d_A = 0.05$ mm, $d_B = 2$ mm, and $H_0 = 6500$ Oe, the absorption charts formed by taking $r_0 = 10$ mm, $r_0 = 50$ mm, $r_0 = 100$ mm, and $r_0 = 1$ mm, respectively, as shown in **Figure 8**. For Figure 8a, the widest AB is obtained at $\gamma = 75°$ for $r_0 = 1$ mm. In Figure 8b, the 1-D MFSPCs do not form any ABs at r_0 of 50 mm, and the maximum value of absorptance is ≈0.6, which is much lower than the case where r_0 is 10 mm. In contrast to Figure 8a, although the absorptance of the 1-D MFSPCs with $r_0 = 50$ mm reduces, the trend of the absorptance with the incident angles is generally comparable, and the highest values of the absorptance all arise at large incident angles. It is further demonstrated that a large angle of incidence is essential for the formation of absorption bands. Figure 8c is akin to Figure 8b in that the absorptance declines significantly when r_0 is 100 mm compared to the 1-D MFSPCs with $r_0 = 10$ mm. In this case, r_0 differs from d_A and d_B by several orders of magnitude, and the curvature of the spherical surface can be approximated as infinity. Therefore, the transmission properties of the 1-D MFSPCs are similar to those of the 1-D PPCs. The absorptance is at a low level due to the limitations of the initial radius, dielectric thickness, and frequency setting. For Figure 8d, in the case of r_0 of 1 mm, ABs appear in the γ range from 0° to 89°, with numerous wide ABs formed between the $\gamma = 60°$ and $\gamma = 75°$. Since $r_0 = 1$ mm, which is in the same order of magnitude as d_A and d_B, the transmission properties of the spherical wave are more prominent. The peaks of absorption are not only present in the frequency band with a large incidence angle but also are distributed in all directions. As a whole, the absorption spectra have an identical trend, which is determined by the periodicity of the structure and the nature of the spherical waves. However, different r_0 can obtain ABs located in different frequency bands, and the number of ABs can also be altered by manipulating r_0. When constructing a 1-D MFSPCs structure, in addition to considering the incidence angle, material thickness, and the magnitude of the external magnetic field, determining

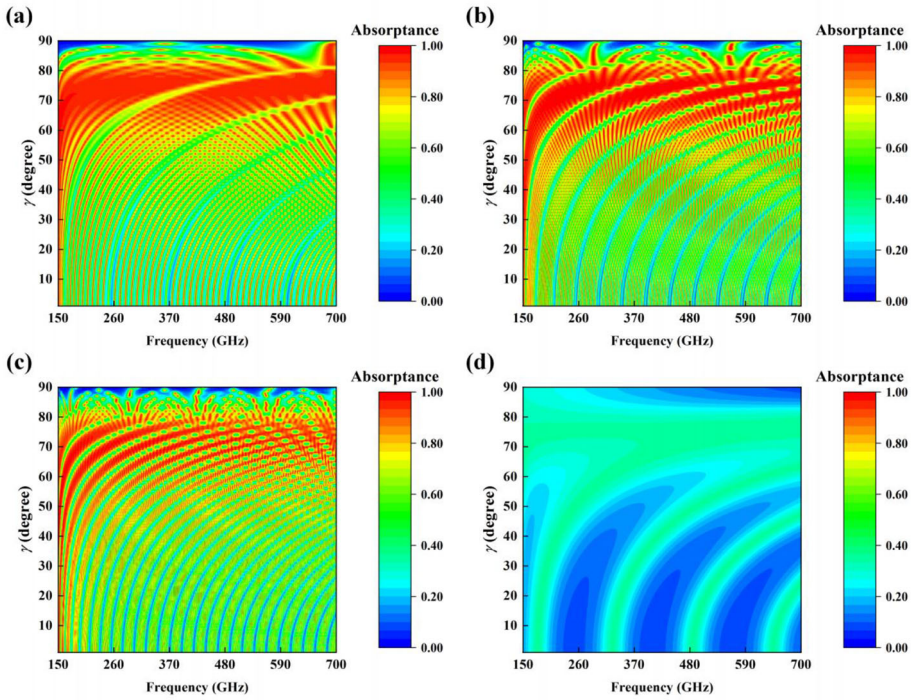

Figure 7. The effects of d_B on the absorption spectra of the TE waves, when $d_A = 0.05$ mm, $r_0 = 1$ cm and $H_0 = 6500$ Oe. a) $d_B = 2$ mm, b) $d_B = 5$ mm, c) $d_B = 1$ mm, and d) $d_B = 0.1$ mm.

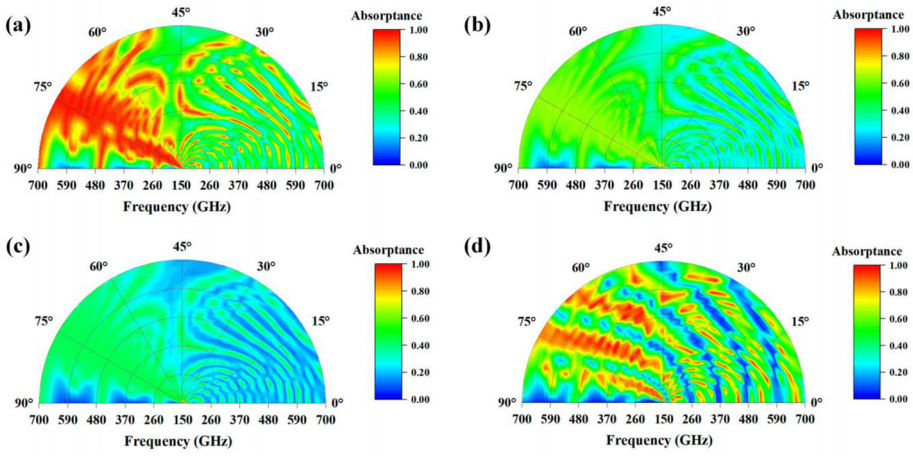

Figure 8. The influences of r_0 on the absorption spectra of the TE waves, when $d_A = 0.05$ mm, $d_B = 2$ mm and $H_0 = 6500$ Oe. a) $r_0 = 10$ mm, b) $r_0 = 50$ mm, c) $r_0 = 100$ mm, and d) $r_0 = 1$ mm.

the appropriate r_0 according to practical needs is also a decisive factor.

4. Conclusion

In summary, a theoretical study of the 1-D MFSPCs is carried out by the TMM. The electric and magnetic field equations of 1-D SPCs are deduced based on the set of Maxwell's equations and the properties of spherical waves. Using the method of solving the spherical Bessel equation, the equation is analyzed theoretically and the expressions for the absorptance, reflectance, and transmittance of the 1-D MFSPCs are derived.

Meanwhile, the 1-D MFSPCs structure is designed to verify the expressions by combining the above-derived transmission property expressions. The structure is formed by the periodic arrangement of the general dielectric and YIG. When $\gamma = 75°$, $r_0 = 1$ mm, $d_A = 0.05$ mm, $d_B = 2$ mm, and $H_0 = 6500$ Oe, such 1-D MFSPCs can form a wide AB between 164.7 and 434.6 GHz and has preeminent absorption performance. The parameters affecting the absorption are also discussed. Unlike the 1-D PPCs, the absorption properties of the 1-D MFSPCs are not only related to the external magnetic field, the incident angle, and the thickness of YIG, but also are closely dependent on the initial radius of the 1-D MFSPCs. The 1-D MFSPCs are tunable and can shift the absorp-

tion spectra to the high-frequency region by boosting the external magnetic field. The magnitudes of d_B and r_0 are not linearly related to the absorptance, and the parameters can be designed according to the actual needs. The ABs of the 1-D MFSPCs not only can alter with the external magnetic field but also by adjusting incidence angle, medium thickness, and initial radius. Manifold absorption spectra can be devised to meet the requirements in different cases, which is the embodiment of the high practicality and flexibility of 1-D SPCs. This research has tremendous potential in the fields of the design of multitasking absorbers and radomes.

Appendix

For matrix M in Equation (49), the specific representation is as follows.

To facilitate the calculation and reading, the transmission matrix of this structure is partitioned and each 4-layer is represented by a matrix, and the total transmission matrix is obtained by multiplying 5 matrices.

$$M_1 = \begin{pmatrix} a_4 \times \begin{pmatrix} a_3 \times (a_1 \times a_2 + b_1 \times c_2) \\ +c_3 \times (a_1 \times b_2 + b_1 \times d_2) \end{pmatrix} & b_4 \times \begin{pmatrix} a_3 \times (a_1 \times a_2 + b_1 \times c_2) \\ +c_3 \times (a_1 \times b_2 + b_1 \times d_2) \end{pmatrix} \\ +c_4 \times \begin{pmatrix} d_3 \times (a_1 \times a_2 + b_1 \times c_2) \\ +d_3 \times (a_1 \times b_2 + b_1 \times d_2) \end{pmatrix} & +d_4 \times \begin{pmatrix} d_3 \times (a_1 \times a_2 + b_1 \times c_2) \\ +d_3 \times (a_1 \times b_2 + b_1 \times d_2) \end{pmatrix} \\ a_4 \times \begin{pmatrix} a_3 \times (a_2 \times c_1 + c_2 \times d_1) \\ +c_3 \times (b_2 \times c_1 + d_1 \times d_2) \end{pmatrix} & b_4 \times \begin{pmatrix} a_3 \times (a_2 \times c_1 + c_2 \times d_1) \\ +c_3 \times (b_2 \times c_1 + d_1 \times d_2) \end{pmatrix} \\ +c_4 \times \begin{pmatrix} d_3 \times (a_2 \times c_1 + c_2 \times d_1) \\ +d_3 \times (b_2 \times c_1 + d_1 \times d_2) \end{pmatrix} & +d_4 \times \begin{pmatrix} d_3 \times (a_2 \times c_1 + c_2 \times d_1) \\ +d_3 \times (b_2 \times c_1 + d_1 \times d_2) \end{pmatrix} \end{pmatrix} \tag{A1}$$

$$M_2 = \begin{pmatrix} a_8 \times \begin{pmatrix} a_7 \times (a_5 \times a_6 + b_5 \times c_6) \\ +c_7 \times (a_5 \times b_6 + b_5 \times d_6) \end{pmatrix} & b_8 \times \begin{pmatrix} a_7 \times (a_5 \times a_6 + b_5 \times c_6) \\ +c_7 \times (a_5 \times b_6 + b_5 \times d_6) \end{pmatrix} \\ +c_8 \times \begin{pmatrix} b_7 \times (a_5 \times a_6 + b_5 \times c_6) \\ +d_7 \times (a_5 \times b_6 + b_5 \times d_6) \end{pmatrix} & +d_8 \times \begin{pmatrix} b_7 \times (a_5 \times a_6 + b_5 \times c_6) \\ +d_7 \times (a_5 \times b_6 + b_5 \times d_6) \end{pmatrix} \\ a_8 \times \begin{pmatrix} a_7 \times (a_6 \times c_5 + c_6 \times d_5) \\ +c_7 \times (b_6 \times c_5 + d_5 \times d_6) \end{pmatrix} & b_8 \times \begin{pmatrix} a_7 \times (a_6 \times c_5 + c_6 \times d_5) \\ +c_7 \times (b_6 \times c_5 + d_5 \times d_6) \end{pmatrix} \\ +c_8 \times \begin{pmatrix} b_7 \times (a_6 \times c_5 + c_6 \times d_5) \\ +d_7 \times (b_6 \times c_5 + d_5 \times d_6) \end{pmatrix} & +d_8 \times \begin{pmatrix} b_7 \times (a6 \times c_5 + c_6 \times d_5) \\ +d_7 \times (b_6 \times c_5 + d_5 \times d_6) \end{pmatrix} \end{pmatrix} \tag{A2}$$

$$M_3 = \begin{pmatrix} a_{12} \times \begin{pmatrix} a_{11} \times (a_9 \times a_{10} + b_9 \times c_{10}) \\ +c_{11} \times (a_9 \times b_{10} + b_9 \times d_{10}) \end{pmatrix} & b_{12} \times \begin{pmatrix} a_{11} \times (a_9 \times a_{10} + b_9 \times c_{10}) \\ +c_{11} \times (a_9 \times b_{10} + b_9 \times d_{10}) \end{pmatrix} \\ +c_{12} \times \begin{pmatrix} b_{11} \times (a_9 \times a_{10} + b_9 \times c_{10}) \\ +d_{11} \times (a_9 \times b_{10} + b_9 \times d_{10}) \end{pmatrix} & +d_{12} \times \begin{pmatrix} b_{11} \times (a_9 \times a_{10} + b_9 \times c_{10}) \\ +d_{11} \times (a_9 \times b_{10} + b_9 \times d_{10}) \end{pmatrix} \\ a_{12} \times \begin{pmatrix} a_{11} \times (a_{10} \times c_9 + c_{10} \times d_9) \\ +c_{11} \times (b_{10} \times c_9 + d_9 \times d_{10}) \end{pmatrix} & b_{12} \times \begin{pmatrix} a_{11} \times (a_{10} \times c_9 + c_{10} \times d_9) \\ +c_{11} \times (b_{10} \times c_9 + d_9 \times d_{10}) \end{pmatrix} \\ +c_{12} \times \begin{pmatrix} b_{11} \times (a_{10} \times c_9 + c_{10} \times d_9) \\ +d_{11} \times (b_{10} \times c_9 + d_9 \times d_{10}) \end{pmatrix} & +d_{12} \times \begin{pmatrix} b_{11} \times (a_{10} \times c_9 + c_{10} \times d_9) \\ +d_{11} \times (b_{10} \times c_9 + d_9 \times d_{10}) \end{pmatrix} \end{pmatrix} \tag{A3}$$

$$M_4 = \begin{pmatrix} a_{16} \times \begin{pmatrix} a_{15} \times (a_{13} \times a_{14} + b_{13} \times c_{14}) \\ +c_{15} \times (a_{13} \times b_{14} + b_{13} \times d_{14}) \end{pmatrix} & b_{16} \times \begin{pmatrix} a_{15} \times (a_{13} \times a_{14} + b_{13} \times c_{14}) \\ +c_{15} \times (a_{13} \times b_{14} + b_{13} \times d_{14}) \end{pmatrix} \\ +c_{16} \times \begin{pmatrix} b_{15} \times (a_{13} \times a_{14} + b_{13} \times c_{14}) \\ +d_{15} \times (a_{13} \times b_{14} + b_{13} \times d_{14}) \end{pmatrix} & +d_{16} \times \begin{pmatrix} b_{15} \times (a_{13} \times a_{14} + b_{13} \times c_{14}) \\ +d_{15} \times (a_{13} \times b_{14} + b_{13} \times d_{14}) \end{pmatrix} \\ a_{16} \times \begin{pmatrix} a_{15} \times (a_{14} \times c_{13} + c_{14} \times d_{13}) \\ +c_{15} \times (b_{14} \times c_{13} + d_{13} \times d_{14}) \end{pmatrix} & b_{16} \times \begin{pmatrix} a_{15} \times (a_{14} \times c_{13} + c_{14} \times d_{13}) \\ +c_{15} \times (b_{14} \times c_{13} + d_{13} \times d_{14}) \end{pmatrix} \\ +c_{16} \times \begin{pmatrix} b_{15} \times (a_{14} \times c_{13} + c_{14} \times d_{13}) \\ +d_{15} \times (b_{14} \times c_{13} + d_{13} \times d_{14}) \end{pmatrix} & +d_{16} \times \begin{pmatrix} b_{15} \times (a_{14} \times c_{13} + c_{14} \times d_{13}) \\ +d_{15} \times (b_{14} \times c_{13} + d_{13} \times d_{14}) \end{pmatrix} \end{pmatrix} \tag{A4}$$

$$M_5 = \begin{pmatrix} a_{20} \times \begin{pmatrix} a_{19} \times (a_{17} \times a_{18} + b_{17} \times c_{18}) \\ +c_{19} \times (a_{17} \times b_{18} + b_{17} \times d_{18}) \end{pmatrix} & b_{20} \times \begin{pmatrix} a_{19} \times (a_{17} \times a_{18} + b_{17} \times c_{18}) \\ +c_{19} \times (a_{17} \times b_{18} + b_{17} \times d_{18}) \end{pmatrix} \\ +c_{20} \times \begin{pmatrix} b_{19} \times (a_{17} \times a_{18} + b_{17} \times c_{18}) \\ +d_{19} \times (a_{17} \times b_{18} + b_{17} \times d_{18}) \end{pmatrix} & +d_{20} \times \begin{pmatrix} b_{19} \times (a_{17} \times a_{18} + b_{17} \times c_{18}) \\ +d_{19} \times (a_{17} \times b_{18} + b_{17} \times d_{18}) \end{pmatrix} \\ a_{20} \times \begin{pmatrix} a_{19} \times (a_{18} \times c_{17} + c_{18} \times d_{17}) \\ +c_{19} \times (b_{18} \times c_{17} + d_{17} \times d_{18}) \end{pmatrix} & b_{20} \times \begin{pmatrix} a_{19} \times (a_{18} \times c_{17} + c_{18} \times d_{17}) \\ +c_{19} \times (b_{18} \times c_{17} + d_{17} \times d_{18}) \end{pmatrix} \\ +c_{20} \times \begin{pmatrix} b_{19} \times (a_{18} \times c_{17} + c_{18} \times d_{17}) \\ +d_{19} \times (b_{18} \times c_{17} + d_{17} \times d_{18}) \end{pmatrix} & +d_{20} \times \begin{pmatrix} b_{19} \times (a_{18} \times c_{17} + c_{18} \times d_{17}) \\ +d_{19} \times (b_{18} \times c_{17} + d_{17} \times d_{18}) \end{pmatrix} \end{pmatrix} \tag{A5}$$

$$M^{-1} = M_1 \times M_2 \times M_3 \times M_4 \times M_5 \tag{A6}$$

The detailed expressions for each element are as follows.

$$a_1 = \frac{j_l(k_1 r_1)}{j_l(k_1 r_0)\, n'_l(k_1 r_0) - n_l(k_1 r_0)\, j_l'(k_1 r_0)} \left[n_l'(k_1 r_0) + \frac{n_l(k_1 r_0)}{k_1 r_0} \right] + \frac{n_l(k_1 r_1)}{n_l(k_1 r_0)\, j_l'(k_1 r_0) - n'_l(k_1 r_0)\, j_l(k_1 r_0)} \left[j_l'(k_1 r_0) + \frac{j_l(k_1 r_0)}{k_1 r_0} \right] \tag{A7}$$

$$a_2 = \frac{j_l(k_2 r_2)}{j_l(k_2 r_1)\, n'_l(k_2 r_1) - n_l(k_2 r_1)\, j_l'(k_2 r_1)} \left[n_l'(k_2 r_1) + \frac{n_l(k_2 r_1)}{k_2 r_1} \right] + \frac{n_l(k_2 r_2)}{n_l(k_2 r_1)\, j_l'(k_2 r_1) - n'_l(k_2 r_1)\, j_l(k_2 r_1)} \left[j_l'(k_2 r_1) + \frac{j_l(k_2 r_1)}{k_2 r_1} \right] \tag{A8}$$

$$a_3 = \frac{j_l(k_1 r_3)}{j_l(k_1 r_2)\, n'_l(k_1 r_2) - n_l(k_1 r_2)\, j_l'(k_1 r_2)} \left[n_l'(k_1 r_2) + \frac{n_l(k_1 r_2)}{k_1 r_2} \right] + \frac{n_l(k_1 r_3)}{n_l(k_1 r_2)\, j_l'(k_1 r_2) - n'_l(k_1 r_2)\, j_l(k_1 r_2)} \left[j_l'(k_1 r_2) + \frac{j_l(k_1 r_2)}{k_1 r_2} \right] \tag{A9}$$

.....

$$a_{19} = \frac{j_l(k_1 r_{19})}{j_l(k_1 r_{18})\, n'_l(k_1 r_{18}) - n_l(k_1 r_{18})\, j_l'(k_1 r_{18})} \left[n_l'(k_1 r_{18}) + \frac{n_l(k_1 r_{18})}{k_1 r_{18}} \right] + \frac{n_l(k_1 r_{19})}{n_l(k_1 r_{18})\, j_l'(k_1 r_{18}) - n'_l(k_1 r_{18})\, j_l(k_1 r_{18})} \left[j_l'(k_1 r_{18}) + \frac{j_l(k_1 r_{18})}{k_1 r_{18}} \right] \tag{A10}$$

$$a_{20} = \frac{j_l(k_2 r_{20})}{j_l(k_2 r_{19})\, n'_l(k_2 r_{19}) - n_l(k_2 r_{19})\, j_l'(k_2 r_{19})} \left[n_l'(k_2 r_{19}) + \frac{n_l(k_2 r_{19})}{k_2 r_{19}} \right] + \frac{n_l(k_2 r_{20})}{n_l(k_2 r_{19})\, j_l'(k_2 r_{19}) - n'_l(k_2 r_{19})\, j_l(k_2 r_{19})} \left[j_l'(k_2 r_{19}) + \frac{j_l(k_2 r_{19})}{k_2 r_{19}} \right] \tag{A11}$$

In summary, based on the results obtained from the TMM calculations, the generic expression for the matrix element a_n is:

$$a_n = \frac{j_l(k_{1/2} r_n)}{j_l(k_{1/2} r_{n-1})\, n'_l(k_{1/2} r_{n-1}) - n_l(k_{1/2} r_{n-1})\, j_l'(k_{1/2} r_{n-1})} \left[n_l'(k_{1/2} r_{n-1}) + \frac{n_l(x_{n-1})}{k_{1/2} r_{n-1}} \right] + \frac{n_l(k_{1/2} r_n)}{n_l(k_{1/2} r_{n-1})\, j_l'(k_{1/2} r_{n-1}) - n'_l(k_{1/2} r_{n-1})\, j_l(k_{1/2} r_{n-1})} \left[j_l'(k_{1/2} r_{n-1}) + \frac{j_l(k_{1/2} r_{n-1})}{k_{1/2} r_{n-1}} \right] \tag{A12}$$

where n is taken from 1 to 20, corresponding to the nth layer of the medium from the inside out, and $j_l(k_{1/2}r_n)$, $j_l'(k_{1/2}r_n)$, $n_l(k_{1/2}r_n)$, and $n_l'(k_{1/2}r_n)$ are the spherical Bessel functions and their first order derivatives, which are not expanded here. Regarding the structure of 1-D MFSPCs constructed in this paper, for example, $k_1 = \omega/c \cdot n_p \cdot \cos\gamma_1$ is chosen as the wave vector when n is odd, and $\boldsymbol{k_2}$ is chosen as the wave vector when n is even$k_2 = \omega\sqrt{\varepsilon_0 \varepsilon_m \mu_0 \mu_{eff}} \cdot \cos\gamma_2 = \omega/c \cdot n_{TE} \cdot \cos\gamma_2$. To add, here γ_1 is the angle of incidence and γ_2 can be calculated by Fresnel's theorem.

The magnetic field magnitude H_0 is contained in $\boldsymbol{k_2}$, which is related to μ_{eff}. The specific relationships are as follows.

$$\mu_{eff} = \left[\mu_r^2 + (i\mu_k)^2 \right] / \mu_r \tag{A13}$$

$$\mu_r = 1 + \frac{\omega_m(\omega_0 - i\eta\omega)}{(\omega_0 - i\eta\omega)^2 - \omega^2} \tag{A14}$$

$$\mu_k = \frac{\omega_m \omega}{(\omega_0 - i\eta\omega)^2 - \omega^2} \tag{A15}$$

$\omega_0 = 2\pi f_0$ is the resonance frequency with $f_0 = 2.8 \times 10^6 \times H_0$. It can be understood that the parameters γ, and H_0 are related to the wave vector $\boldsymbol{k_2}$, and changing the parameters is an adjustment of $\boldsymbol{k_2}$, which in turn affects the overall absorption spectra.

Homoplastically,

$$b_1 = \frac{j_l(k_1 r_1)}{n_l(k_1 r_0)\, j_l'(k_1 r_0) - n'_l(k_1 r_0)\, j_l(k_1 r_0)} \left[-\frac{i\omega\mu_0}{k_1} n_l(k_1 r_0) \right] + \frac{n_l(k_1 r_1)}{j_l(k_1 r_0)\, n'_l(k_1 r_0) - n_l(k_1 r_0)\, j_l'(k_1 r_0)} \left[-\frac{i\omega\mu_0}{k_1} j_l(k_1 r_0) \right] \tag{A16}$$

$$b_2 = \frac{j_l(k_2 r_2)}{n_l(k_2 r_1)\, j_l'(k_2 r_1) - n'_l(k_2 r_1)\, j_l(k_2 r_1)} \left[-\frac{i\omega\mu_0}{k_2} n_l(k_2 r_1) \right] + \frac{n_l(k_2 r_2)}{j_l(k_2 r_1)\, n'_l(k_2 r_1) - n_l(k_2 r_1)\, j_l'(k_2 r_1)} \left[-\frac{i\omega\mu_0}{k_2} j_l(k_2 r_1) \right] \tag{A17}$$

$$b_3 = \frac{j_l(k_1 r_3)}{n_l(k_1 r_2)\, j_l'(k_1 r_2) - n'_l(k_1 r_2)\, j_l(k_1 r_2)} \left[-\frac{i\omega\mu_0}{k_1} n_l(k_1 r_2) \right] + \frac{n_l(k_1 r_3)}{j_l(k_1 r_2)\, n'_l(k_1 r_2) - n_l(k_1 r_2)\, j_l'(k_1 r_2)} \left[-\frac{i\omega\mu_0}{k_1} j_l(k_1 r_2) \right] \tag{A18}$$

.....

$$b_{19} = \frac{j_l(k_1 r_{19})}{n_l(k_1 r_{18})\, j_l'(k_1 r_{18}) - n'_l(k_1 r_{18})\, j_l(k_1 r_{18})} \left[-\frac{i\omega\mu_0}{k_1} n_l(k_1 r_{18}) \right] + \frac{n_l(k_1 r_{19})}{j_l(k_1 r_{18})\, n'_l(k_1 r_{18}) - n_l(k_1 r_{18})\, j_l'(k_1 r_{18})} \left[-\frac{i\omega\mu_0}{k_1} j_l(k_1 r_{18}) \right] \tag{A19}$$

$$b_{20} = \frac{j_l(k_2 r_{20})}{n_l(k_2 r_{19})\, j_l'(k_2 r_{19}) - n'_l(k_2 r_{19})\, j_l(k_2 r_{19})} \left[-\frac{i\omega\mu_0}{k_2} n_l(k_2 r_{19}) \right] + \frac{n_l(k_2 r_{20})}{j_l(k_2 r_{19})\, n'_l(k_2 r_{19}) - n_l(k_2 r_{19})\, j_l'(k_2 r_{19})} \left[-\frac{i\omega\mu_0}{k_2} j_l(k_2 r_{19}) \right] \tag{A20}$$

The formula for the general term of b_n is:

$$b_n = \frac{j_l(k_{1/2} r_n)}{n_l(k_{1/2} r_{n-1})\, j_l'(k_{1/2} r_{n-1}) - n'_l(k_{1/2} r_{n-1})\, j_l(k_{1/2} r_{n-1})} \left[-\frac{i\omega\mu_0}{k_{1/2}} n_l(k_{1/2} r_{n-1}) \right] + \frac{n_l(k_{1/2} r_n)}{j_l(k_{1/2} r_{n-1})\, n'_l(k_{1/2} r_{n-1}) - n_l(k_{1/2} r_{n-1})\, j_l'(k_{1/2} r_{n-1})} \left[-\frac{i\omega\mu_0}{k_{1/2}} j_l(k_{1/2} r_{n-1}) \right] \tag{A21}$$

The selections and definitions of n and $\boldsymbol{k}$ in Equation (A12) are the same as in the a_n case.

Finally,

$$c_1 = -\frac{1}{i\omega\mu_0 r_1}\left\{\frac{j_l(k_1r_1)}{j_l(k_1r_0)\,n'_l(k_1r_0)-n_l(k_1r_0)j_l'(k_1r_0)}\left[n_l'(k_1r_0)+\frac{n_l(k_1r_0)}{k_1r_0}\right]+\frac{n_l(k_1r_1)}{n_l(k_1r_0)j_l'(k_1r_0)-n'_l(k_1r_0)j_l(k_1r_0)}\left[j_l'(k_1r_0)+\frac{j_l(k_1r_0)}{k_1r_0}\right]\right.$$
$$\left.+\frac{k_1r_1j_l'(k_1r_1)}{j_l(k_1r_0)\,n'_l(k_1r_0)-n_l(k_1r_0)j_l'(k_1r_0)}\left[n_l'(k_1r_0)+\frac{n_l(k_1r_0)}{k_1r_0}\right]+\frac{k_1r_1n_l'(k_1r_1)}{n_l(k_1r_0)j_l'(k_1r_0)-n'_l(k_1r_0)j_l(k_1r_0)}\left[j_l'(k_1r_0)+\frac{j_l(k_1r_0)}{k_1r_0}\right]\right\} \tag{A22}$$

$$c_2 = -\frac{1}{i\omega\mu_0 r_2}\left\{\frac{j_l(k_2r_2)}{j_l(k_2r_1)\,n'_l(k_2r_1)-n_l(k_2r_1)j_l'(k_2r_1)}\left[n_l'(k_2r_1)+\frac{n_l(k_2r_1)}{k_2r_1}\right]+\frac{n_l(k_2r_2)}{n_l(k_2r_1)j_l'(k_2r_1)-n'_l(k_2r_1)j_l(k_2r_1)}\left[j_l'(k_2r_1)+\frac{j_l(k_1r_0)}{k_1r_0}\right]\right.$$
$$\left.+\frac{k_2r_2j_l'(k_2r_2)}{j_l(k_2r_1)\,n'_l(k_2r_1)-n_l(k_2r_1)j_l'(k_2r_1)}\left[n_l'(k_2r_1)+\frac{n_l(k_2r_1)}{k_2r_1}\right]+\frac{k_2r_2n_l'(k_2r_2)}{n_l(k_2r_1)j_l'(k_2r_1)-n'_l(k_2r_1)j_l(k_2r_1)}\left[j_l'(k_2r_1)+\frac{j_l(k_2r_1)}{k_2r_1}\right]\right\} \tag{A23}$$

$$c_3 = -\frac{1}{i\omega\mu_0 r_3}\left\{\frac{j_l(k_1r_3)}{j_l(k_1r_2)\,n'_l(k_1r_2)-n_l(k_1r_2)j_l'(k_1r_2)}\left[n_l'(k_1r_2)+\frac{n_l(k_1r_2)}{k_1r_2}\right]+\frac{n_l(k_1r_3)}{n_l(k_1r_2)j_l'(k_1r_2)-n'_l(k_1r_2)j_l(k_1r_2)}\left[j_l'(k_1r_2)+\frac{j_l(k_1r_2)}{k_1r_2}\right]\right.$$
$$\left.+\frac{k_1r_3j_l'(k_1r_3)}{j_l(k_1r_2)\,n'_l(k_1r_2)-n_l(k_1r_2)j_l'(k_1r_2)}\left[n_l'(k_1r_2)+\frac{n_l(k_1r_2)}{k_1r_2}\right]+\frac{k_1r_3n_l'(k_1r_3)}{n_l(k_1r_2)j_l'(k_1r_2)-n'_l(k_1r_2)j_l(k_1r_2)}\left[j_l'(k_1r_2)+\frac{j_l(k_1r_2)}{k_1r_2}\right]\right\} \tag{A24}$$

.....

$$c_{19} = -\frac{1}{i\omega\mu_0 r_{19}}\left\{\frac{j_l(k_1r_{19})}{j_l(k_1r_{18})\,n'_l(k_1r_{18})-n_l(k_1r_{18})j_l'(k_1r_{18})}\left[n_l'(k_1r_{18})+\frac{n_l(k_1r_{18})}{k_1r_{18}}\right]+\frac{n_l(k_1r_{19})}{n_l(k_1r_{18})j_l'(k_1r_{18})-n'_l(k_1r_{18})j_l(k_1r_{18})}\left[j_l'(k_1r_{18})+\frac{j_l(k_1r_{18})}{k_1r_{18}}\right]\right.$$
$$\left.+\frac{k_1r_{19}j_l'(k_1r_{19})}{j_l(k_1r_{18})\,n'_l(k_1r_{18})-n_l(k_1r_{18})j_l'(k_1r_{18})}\left[n_l'(k_1r_{18})+\frac{n_l(k_1r_{18})}{k_1r_{18}}\right]+\frac{k_1r_{19}n_l'(k_1r_{19})}{n_l(k_1r_{18})j_l'(k_1r_{18})-n'_l(k_1r_{18})j_l(k_1r_{18})}\left[j_l'(k_1r_{18})+\frac{j_l(k_1r_{18})}{k_1r_{18}}\right]\right\} \tag{A25}$$

$$c_{20} = -\frac{1}{i\omega\mu_0 r_{20}}\left\{\frac{j_l(k_2r_{20})}{j_l(k_2r_{19})\,n'_l(k_2r_{19})-n_l(k_2r_{19})j_l'(k_2r_{19})}\left[n_l'(k_2r_{19})+\frac{n_l(k_2r_{19})}{k_2r_{19}}\right]+\frac{n_l(k_2r_{19})}{n_l(k_2r_{19})j_l'(k_2r_{19})-n'_l(k_2r_{19})j_l(k_2r_{19})}\left[j_l'(k_2r_{19})+\frac{j_l(k_2r_{19})}{k_2r_{19}}\right]\right.$$
$$\left.+\frac{k_2r_{20}j_l'(k_2r_{20})}{j_l(k_2r_{19})\,n'_l(k_2r_{19})-n_l(k_2r_{19})j_l'(k_2r_{19})}\left[n_l'(k_2r_{19})+\frac{n_l(k_2r_{19})}{k_2r_{19}}\right]+\frac{k_2r_{20}n_l'(k_2r_{20})}{n_l(k_2r_{19})j_l'(k_2r_{19})-n'_l(k_2r_{19})j_l(k_2r_{19})}\left[j_l'(k_2r_{19})+\frac{j_l(k_2r_{19})}{k_2r_{19}}\right]\right\} \tag{A26}$$

c_n is available as:

$$\begin{aligned}c_n = -\frac{1}{i\omega\mu_0 r_n}\Bigg\{&\frac{j_l(k_2r_{20})}{j_l(k_{1/2}r_{n-1})\,n'_l(k_{1/2}r_{n-1})-n_l(k_{1/2}r_{n-1})j_l'(k_{1/2}r_{n-1})}\left[n_l'(k_{1/2}r_{n-1})+\frac{n_l(k_{1/2}r_{n-1})}{k_{1/2}r_{n-1}}\right]\\&+\frac{n_l(k_{1/2}r_{n-1})}{n_l(k_{1/2}r_{n-1})j_l'(k_{1/2}r_{n-1})-n'_l(k_{1/2}r_{n-1})j_l(k_{1/2}r_{n-1})}\left[j_l'(k_{1/2}r_{n-1})+\frac{j_l(k_{1/2}r_{n-1})}{k_{1/2}r_{n-1}}\right]\\&+\frac{k_{1/2}r_nj_l'(k_{1/2}r_n)}{j_l(k_{1/2}r_{n-1})\,n'_l(k_{1/2}r_{n-1})-n_l(k_{1/2}r_{n-1})j_l'(k_{1/2}r_{n-1})}\left[n_l'(k_{1/2}r_{n-1})+\frac{n_l(k_{1/2}r_{n-1})}{k_{1/2}r_{n-1}}\right]\\&+\frac{k_{1/2}r_nn_l'(k_{1/2}r_n)}{n_l(k_{1/2}r_{n-1})j_l'(k_{1/2}r_{n-1})-n'_l(k_{1/2}r_{n-1})j_l(k_{1/2}r_{n-1})}\left[j_l'(k_{1/2}r_{n-1})+\frac{j_l(k_{1/2}r_{n-1})}{k_{1/2}r_{n-1}}\right]\Bigg\}\end{aligned} \tag{A27}$$

In the same way,

$$d_1 = -\frac{1}{i\omega\mu_0 r_1}\left\{\frac{j_l(k_1r_1)}{n_l(k_1r_0)j_l'(k_1r_0)-n'_l(k_1r_0)j_l(k_1r_0)}\left[-\frac{i\omega\mu_0}{k_1}n_l(k_1r_0)\right]+\frac{n_l(k_1r_1)}{j_l(k_1r_0)n'_l(k_1r_0)-n_l(k_1r_0)j_l'(k_1r_0)}\left[-\frac{i\omega\mu_0}{k_1}j_l(k_1r_0)\right]\right.$$
$$\left.+\frac{k_1r_1j_l'(k_1r_1)}{n_l(k_1r_0)j_l'(k_1r_0)-n'_l(k_1r_0)j_l(k_1r_0)}\left[-\frac{i\omega\mu_0}{k_1}n_l(k_1r_0)\right]+\frac{k_1r_1n_l'(k_1r_1)}{j_l(k_1r_0)n'_l(k_1r_0)-n_l(k_1r_0)j_l'(k_1r_0)}\left[-\frac{i\omega\mu_0}{k_1}j_l(k_1r_0)\right]\right\} \tag{A28}$$

$$d_2 = -\frac{1}{i\omega\mu_0 r_2}\left\{\frac{j_l(k_2r_2)}{n_l(k_2r_1)j_l'(k_2r_1)-n'_l(k_2r_1)j_l(k_2r_1)}\left[-\frac{i\omega\mu_0}{k_2}n_l(k_2r_1)\right]+\frac{n_l(k_2r_2)}{j_l(k_2r_1)n'_l(k_2r_1)-n_l(k_2r_1)j_l'(k_2r_1)}\left[-\frac{i\omega\mu_0}{k_2}j_l(k_2r_1)\right]\right.$$
$$\left.+\frac{k_2r_2j_l'(k_2r_2)}{n_l(k_2r_1)j_l'(k_2r_1)-n'_l(k_2r_1)j_l(k_2r_1)}\left[-\frac{i\omega\mu_0}{k_2}n_l(k_2r_1)\right]+\frac{k_2r_2n_l'(k_2r_2)}{j_l(k_2r_1)n'_l(k_2r_1)-n_l(k_2r_1)j_l'(k_2r_1)}\left[-\frac{i\omega\mu_0}{k_2}j_l(k_2r_1)\right]\right\} \tag{A29}$$

$$d_3 = -\frac{1}{i\omega\mu_0 r_3}\left\{\frac{j_l(k_1r_3)}{n_l(k_1r_2)j_l'(k_1r_2)-n'_l(k_1r_2)j_l(k_1r_2)}\left[-\frac{i\omega\mu_0}{k_1}n_l(k_1r_2)\right]+\frac{n_l(k_1r_3)}{j_l(k_1r_2)n'_l(k_1r_2)-n_l(k_1r_2)j_l'(k_1r_2)}\left[-\frac{i\omega\mu_0}{k_1}j_l(k_1r_2)\right]\right.$$
$$\left.+\frac{k_1r_3j_l'(k_1r_3)}{n_l(k_1r_2)j_l'(k_1r_2)-n'_l(k_1r_2)j_l(k_1r_2)}\left[-\frac{i\omega\mu_0}{k_1}n_l(k_1r_2)\right]+\frac{k_1r_3n_l'(k_1r_3)}{j_l(k_1r_2)n'_l(k_1r_2)-n_l(k_1r_2)j_l'(k_1r_2)}\left[-\frac{i\omega\mu_0}{k_1}j_l(k_1r_2)\right]\right\} \tag{A30}$$

.....

$$d_{19} = -\frac{1}{i\omega\mu_0 r_{19}}\left\{\frac{j_l(k_1r_{19})}{n_l(k_1r_{18})j_l'(k_1r_{18})-n'_l(k_1r_{18})j_l(k_1r_{18})}\left[-\frac{i\omega\mu_0}{k_1}n_l(k_1r_{18})\right]+\frac{n_l(k_1r_{19})}{j_l(k_1r_{18})n'_l(k_1r_{18})-n_l(k_1r_{18})j_l'(k_1r_{18})}\left[-\frac{i\omega\mu_0}{k_1}j_l(k_1r_{18})\right]\right.$$
$$\left.+\frac{k_1r_1j_l'(k_1r_{19})}{n_l(k_1r_{18})j_l'(k_1r_{18})-n'_l(k_1r_{18})j_l(k_1r_{18})}\left[-\frac{i\omega\mu_0}{k_1}n_l(k_1r_{18})\right]+\frac{k_1r_{19}n_l'(k_1r_{19})}{j_l(k_1r_{18})n'_l(k_1r_{18})-n_l(k_1r_{18})j_l'(k_1r_{18})}\left[-\frac{i\omega\mu_0}{k_1}j_l(k_1r_{18})\right]\right\} \tag{A31}$$

$$d_{20} = -\frac{1}{i\omega\mu_0 r_{20}}\left\{\frac{j_l(k_2r_{20})}{n_l(k_2r_{19})j_l'(k_2r_{19})-n'_l(k_2r_{19})j_l(k_2r_{19})}\left[-\frac{i\omega\mu_0}{k_2}n_l(k_2r_{19})\right]+\frac{n_l(k_2r_{20})}{j_l(k_2r_{19})n'_l(k_2r_{19})-n_l(k_2r_{19})j_l'(k_2r_{19})}\left[-\frac{i\omega\mu_0}{k_2}j_l(k_2r_{19})\right]\right.$$
$$\left.+\frac{k_2r_{20}j_l'(k_2r_{20})}{n_l(k_2r_{19})j_l'(k_2r_{19})-n'_l(k_2r_{19})j_l(k_2r_{19})}\left[-\frac{i\omega\mu_0}{k_2}n_l(k_2r_{19})\right]+\frac{k_2r_{20}n_l'(k_2r_{20})}{j_l(k_2r_{19})n'_l(k_2r_{19})-n_l(k_2r_{19})j_l'(k_2r_{19})}\left[-\frac{i\omega\mu_0}{k_2}j_l(k_2r_{19})\right]\right\} \tag{A32}$$

d_n can be written as:

$$d_n = -\frac{1}{i\omega\mu_0 r_n}\left\{\frac{j_l(k_{1/2}r_n)}{n_l(k_{1/2}r_{n-1})j_l'(k_{1/2}r_{n-1})-n'_l(k_{1/2}r_{n-1})j_l(k_{1/2}r_{n-1})}\left[-\frac{i\omega\mu_0}{k_{1/2}}n_l(k_{1/2}r_{n-1})\right]\right.$$
$$+\frac{n_l(k_{1/2}r_n)}{j_l(k_{1/2}r_{n-1})n'_l(k_{1/2}r_{n-1})-n_l(k_{1/2}r_{n-1})j_l'(k_{1/2}r_{n-1})}\left[-\frac{i\omega\mu_0}{k_{1/2}}j_l(k_{1/2}r_{n-1})\right]$$
$$+\frac{k_{1/2}r_nj_l'(k_{1/2}r_n)}{n_l(k_{1/2}r_{n-1})j_l'(k_{1/2}r_{n-1})-n'_l(k_{1/2}r_{n-1})j_l(k_{1/2}r_{n-1})}\left[-\frac{i\omega\mu_0}{k_{1/2}}n_l(k_{1/2}r_{n-1})\right]$$
$$\left.+\frac{k_{1/2}r_nn_l'(k_{1/2}r_n)}{j_l(k_{1/2}r_{n-1})n'_l(k_{1/2}r_{n-1})-n_l(k_{1/2}r_{n-1})j_l'(k_{1/2}r_{n-1})}\left[-\frac{i\omega\mu_0}{k_{1/2}}j_l(k_{1/2}r_{n-1})\right]\right\} \tag{A33}$$

The definitions of n and $\boldsymbol{k}$ in Equations (A27) and (A33) are identical to Equation (A12).

Acknowledgements

This work was supported by the College Student Innovation Training Program of Nanjing University of Posts and Telecommunications.

Conflict of Interest

The authors declare no conflict of interest.

Data Availability Statement

The data that support the findings of this study are available on request from the corresponding author. The data are not publicly available due to privacy or ethical restrictions.

Keywords

absorption, magnetized ferrite materials, spherical photonic crystals, transfer matrix method

Received: August 4, 2022
Revised: October 6, 2022
Published online:

[1] E. Yablonovitch, *Phys. Rev. Lett.* **1987**, *58*, 2059.
[2] S. John, *Phys. Rev. Lett.* **1987**, *58*, 2486.
[3] C. Sauvan, P. Lalanne, J.-P. Hugonin, *Nature* **2004**, *429*, 6988.
[4] P. E. Barclay, K. Srinivasan, O. Painter, *Opt. Express* **2005**, *13*, 801.
[5] T. Kim, J. W. Lee, C. Park, K. Lee, C. E. Lee, S. Lee, Y. Kim, S. Kim, S. Jeon, D. Y. Ryu, W. G. Koh, C. Park, *Nano Energy* **2022**, *92*, 106688.
[6] B. B. Hong, N. X. Feng, J. Chen, G. P. Wang, D. Viktor, C. Roland, C. John, R. Ian, S. Nutapong, *Opt. Express* **2020**, *28*, 27903.
[7] H. S. Li, M. X. Low, R. Ako, M. Bhaskaran, S. Sriram, W. Withayachumnankul, B. Kuhlmey, S. Atakaramians, *Adv. Mater. Technol.* **2020**, *5*, 2000117.
[8] Z. A. Zaky, A. M. Ahmed, A. H. Aly, A. S. Shalaby, *Sci. Rep.* **2020**, *10*, 9736.
[9] P. Yu, J. Wu, E. Ashalley, A. Govorov, Z. Wang, *J. Phys. D: Appl. Phys.* **2016**, *49*, 365101.
[10] Z. Y. Li, L. L. Lin, *Phys. Rev. E* **2003**, *67*, 46607.
[11] S. A. El-Naggar, *Optik* **2020**, *200*, 163447.
[12] J. A. Fernandes, D. H. A. L. Anselmo, M. S. Vasconcelos, V. D. Mello, *Opt. Mater.* **2021**, *121*, 111566.
[13] J. T. Zhang, S. S. Rao, D. Zhang, H. F. Zhang, *Physica B* **2022**, *639*, 414025.
[14] H. M. Peng, B. F. Wan, P. X. Wang, D. Zhang, H. F. Zhang, *Opt. Quantum Electron.* **2021**, *53*, 256.
[15] C. A. Hu, C. J. Wu, T. J. Yang, S. L. Yang, *Opt. Commun.* **2013**, *291*, 424.
[16] Y. Jiang, H. Jill, *Appl. Opt.* **1994**, *33*, 7431.
[17] Y. Jiang, H. Jill, *Appl. Phys. Lett.* **1993**, *63*, 1453.
[18] X. W. Zhao, W. C. Li, E. D. Gu, L. F. Wang, *Adv. Mater. Technol.* **2013**, *2450*, 302.
[19] T. Larsen, A. Bjarklev, D. Hermann, J. Broeng, *Opt. Express* **2003**, *11*, 2589.
[20] K. Ishizaki, M. De Zoysa, Y. Tanaka, T. Umeda, Y. Kawamoto, S. Noda, *Opt. Express* **2015**, *23*, A1040.
[21] W. L. Moreira, A. A. R. Neves, M. K. Garbos, T. G. Euser, C. L. Cesar, *Opt. Express* **2016**, *24*, 2370.
[22] J. Zhang, Z. Meng, J. Liu, S. Chen, Z. Yu, *ACS Appl. Mater. Interfaces* **2019**, *11*, 42629.
[23] B. G. Xu, D. G. Zhang, Y. Wang, B. B. Hong, G. X. Shu, W. L. He, *Results Phys.* **2022**, *34*, 105315.
[24] K. Wang, C. Li, Z. Li, H. Li, A. Li, K. Li, X. Lai, Q. Liao, F. Xie, M. Li, *Nanoscale* **2019**, *11*, 14147
[25] S. J. Guo, M. Y. Mao, Z. W. Zhou, D. Zhang, H. F. Zhang, *J. Phys. D: Appl. Phys.* **2021**, *54*, 015004.
[26] Y. Wang, D. G. Zhang, S. X. Xu, B. G. Xu, Z. Dong, *Chin. Opt. Lett.* **2017**, *15*, 111601.
[27] J. X. Liu, H. Y. Xu, Z. K. Yang, X. Xie, Y. Zhang, H. W. Yang, *Plasmonics* **2017**, *12* ,971.
[28] H. Mehdian, Z. Mohammadzahery, A. Hasanbeigi, *J. Phys. D: Appl. Phys.* **2015**, *48*, 305101.
[29] V. E. Babicheva, S. V. Zhukovsky, A. V. Lavrinenko, *Opt. Express* **2014**, *22*, 28890.
[30] M. Vaseem, F. A. Ghaffar, M. F. Farooqui, A. Shamim, *Adv. Mater. Technol.* **2018**, *3*, 1700242.
[31] Y. Sharma, S. Prasad, *Eur. Phys. J. D* **2018**, *72*, 543.
[32] A. J. Baden, *Ferrites at Microwave Frequencies*, 2nd ed., Institution of Electrical Engineers, London **1987**.
[33] S. Yogesh, P. Surendra, S. Vivek, *Opt. Quantum Electron.* **2018**, *50*, 2542.
[34] B. K. Zhou, E. W. Li, Y. F. Bo, A. Wang, *J. Lightwave Technol.* **2020**, *38*, 3338.

